Confinement and Lack of Thermalization after Quenches in the Bosonic Schwinger Model

Titas Chanda[,1,*] Jakub Zakrzewski[,1,2] Maciej Lewenstein[,3,4] and Luca Tagliacozzo[5,6]

[1]*Instytut Fizyki Teoretycznej, Uniwersytet Jagielloński, Łojasiewicza 11, 30-348 Kraków, Poland*
[2]*Mark Kac Complex Systems Research Center, Jagiellonian University in Krakow, Łojasiewicza 11, 30-348 Kraków, Poland*
[3]*ICFO-Institut de Ciències Fotòniques, The Barcelona Institute of Science and Technology,*
Av. Carl Friedrich Gauss 3, 08860 Castelldefels (Barcelona), Spain
[4]*ICREA, Passeig Lluis Companys 23, 08010 Barcelona, Spain*
[5]*Department of Physics and SUPA, University of Strathclyde, Glasgow G4 0NG, United Kingdom*
[6]*Department de Física Quàntica i Astrofísica and Institut de Ciències del Cosmos (ICCUB), Universitat de Barcelona,*
Martí i Franquès 1, 08028 Barcelona, Catalonia, Spain

We excite the vacuum of a relativistic theory of bosons coupled to a $U(1)$ gauge field in $1 + 1$ dimensions (bosonic Schwinger model) out of equilibrium by creating a spatially separated particle-antiparticle pair connected by a string of electric field. During the evolution, we observe a strong confinement of bosons witnessed by the bending of their light cone, reminiscent of what has been observed for the Ising model [Nat. Phys. **13**, 246 (2017)]. As a consequence, for the timescales we are able to simulate, the system evades thermalization and generates exotic asymptotic states. These states are made of two disjoint regions, an external deconfined region that seems to thermalize, and an inner core that reveals an area-law saturation of the entanglement entropy.

Introduction.—Solving the out-of-equilibrium dynamics (OED) of large many-body quantum systems becomes exponentially hard when the number of constituents increases beyond a few tens. This fact hinders our understanding of important questions such as the existence of new phases of matter [1–3] and the presence or absence of thermalization [4–7].

Symmetries play a crucial role out of equilibrium as they give rise to conservation laws and continuity equations that can strongly constrain the dynamics [8–10]. Local symmetries can also have strong consequences in the OED since they are responsible for interesting phenomena, such as slow dynamics and localization [11–16].

The simplest system with local symmetries is the fermionic Schwinger model (FSM) [17], the quantum electrodynamics in $1 + 1$ dimensions (1D). The FSM, by now, has been studied extensively with traditional methods [11,18–23] and with tensor-network techniques [24–34]. Despite its simplicity, the FSM shares common features with quantum chromodynamics (QCD), such as a nontrivial vacuum exhibiting chiral symmetry breaking and confinement. In particular, the FSM confinement can be seen emerging from a quadratic perturbation of the sine-Gordon model, producing a similar effect to a magnetic field in the Ising model [35–37].

Here, we consider the OED of the bosonic version of the Schwinger model [17–19] (BSM), since the bosonic versions of well-studied fermionic models can unveil unexpected new phenomena [38–40]. Moreover, the

BSM is easier to realize in experiments with ultracold atoms [41–44] using the tools already available in the labs [45–51].

The Hamiltonian version of the BSM is made by two bosonic species that behave, in the noninteracting regime, as a discretized version of the Klein-Gordon (KG) field
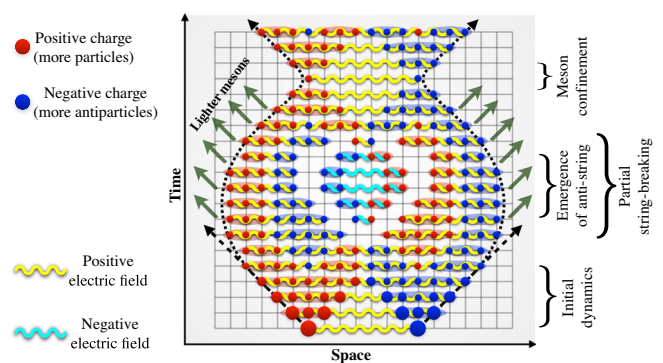

FIG. 1. Semiclassical sketch of the confining dynamics of BSM. We prepare a well-separated pair of particle and antiparticle connected by an electric-flux tube. Initially they start spreading as if they were free, however, their trajectories bend due to the energetic cost of creating larger electric-flux tubes. New dynamical charges are also created during the evolution and partially screen the electric field. Still the electric field oscillates coherently and can form an antistring, creating a central core of strongly correlated bosons. The density of bosons in the core can get depleted through the radiation of lighter mesons that freely propagate.

theory [52–55]. Both species couple to the $U(1)$ field, one representing the particle and the other the antiparticle. The low energy spectrum of this system is always gapped even for massless bosons, and as a result the bosons are always confined [55,56]. By using state-of-the-art matrix-product states (MPS) techniques [64–76] in their gauge-invariant version [24,25,77–82], we analyze the OED in both the massless and the massive regimes of the theory.

We start the OED by creating a particle-antiparticle pair separated by a distance and observe the processes sketched in Fig. 1. The two bosons are connected by an electric-flux tube that bends their trajectories inwards. The process is closer to that observed for the Ising model [83] than to what has been observed in the FSM [30,81].

The initial bosons form a core of a strongly correlated matter that oscillates several times around its original position. Even though, in the small mass regime, the matter density in the core is gradually depleted by the radiation of free lighter mesons, the core stays quantitatively different from the rest of the system, thus keeps a strong memory of the initial state and evades thermalization. The lack of total screening of the electric field by the dynamically generated matter constitutes the main origin of this phenomenon.

However, similar phenomena have been observed in very different contexts such as holographic quenches [84–88], spins systems [11–13], large N gauge theories [16] and quantum link models [14], and Rydberg atoms [89,90]. We thus provide a generic framework to understand such phenomena in terms of entropy production [4,91].

In particular, the lack of homogeneity in space of the classical part of the entanglement entropy provides a generic footprint that allows one to understand the origin of the slow dynamics we observe here and its connection with similar phenomena observed elsewhere.

Model.—The BSM Lagrangian density is given by $\mathcal{L} = -[D_\mu\phi]^*D^\mu\phi - m^2|\phi|^2 - \frac{1}{4}F_{\mu\nu}F^{\mu\nu}$ [92], where ϕ is the complex scalar field, $D_\mu = (\partial_\mu + iqA_\mu)$ is the covariant derivative with q and A_μ being the electronic charge and vector potential, respectively, m is the bare mass of the particles, and $F_{\mu\nu}$ is the electromagnetic field tensor. In 1D, after fixing the temporal gauge, $A_t = 0$, we get the discretized Hamiltonian (in dimensionless units) as [55,56]

$$\hat{H} = \sum_j \hat{L}_j^2 + 2\{x[(m/q)^2 + 2x]\}^{1/2}\sum_j(\hat{a}_j^\dagger\hat{a}_j + \hat{b}_j\hat{b}_j^\dagger)$$
$$- \frac{x^{3/2}}{[(m/q)^2 + 2x]^{1/2}}\sum_j[(\hat{a}_{j+1}^\dagger + \hat{b}_{j+1})\hat{U}_j(\hat{a}_j + \hat{b}_j^\dagger) + \text{H.c.}],$$
$$(1)$$

where $\{\hat{a}_j^\dagger, \hat{a}_j\}$, $\{\hat{b}_j^\dagger, \hat{b}_j\}$ are the bosonic creation-annihilation operators corresponding to charged particles and antiparticles, respectively, $\hat{L}_j$ is the electric field

operator residing on the bond between sites j and $j+1$ with $\{\hat{U}_j, \hat{U}_j^\dagger\}$ being U(1) ladder operators satisfying $[\hat{L}_j, \hat{U}_l] = -\hat{U}_j\delta_{jl}$ and $[\hat{L}_j, \hat{U}_l^\dagger] = \hat{U}_j^\dagger\delta_{jl}$, and $x = 1/(a^2q^2)$ with a being the lattice spacing.

The Hamiltonian is invariant under local $U(1)$ transformations: $\hat{a}_j \to e^{i\alpha_j}\hat{a}_j$, $\hat{b}_j \to e^{-i\alpha_j}\hat{b}_j$, $\hat{U}_j \to e^{-i\alpha_j}\hat{U}_je^{i\alpha_{j+1}}$, where the corresponding Gauss law generators are given by $\hat{G}_j = \hat{L}_j - \hat{L}_{j-1} - \hat{Q}_j$, with $\hat{Q}_j = \hat{a}_j^\dagger\hat{a}_j - \hat{b}_j^\dagger\hat{b}_j$ being the dynamical charge [56]. The physical subspace is spanned by the set of states, $|\Psi\rangle$, that are annihilated by $\hat{G}_j$, i.e., $\hat{G}_j\Psi = 0 \ \forall \ j$. Using this conservation law, in an open chain, one can integrate out the gauge fields using the transformation, $\hat{L}_j = \sum_{l\leq j}\hat{Q}_l$, where we consider the static electric field on the left of the chain to be zero. The effective Hamiltonian for matter fields, once we have integrated out the photons, contains long-range intraspecies repulsion and interspecies attraction.

The continuum limit of the system is achieved by taking the two limits: $N \to \infty$ and $x \to \infty$. However, since our study is motivated by the near future experimental realizations with cold atoms, we consider an open chain made of a finite number of lattice sites $N = 60$ at a fixed value of x that without loss of generality we consider $x = 2$. We obtain systematic matrix-product state approximations to the ground state of the system using the density matrix renormalization group (DMRG) [64,93–95]. This is the starting point for the time evolution, that we approximate by using the time-dependent variational principle (TDVP) [71,72,76,96,97] (see Ref. [56] for more details).

Real-time evolution.—We start the OED of the BSM by creating two extra dynamical charges of opposite signs on the top of the ground state $|\Omega\rangle$ of the Hamiltonian (1). They are located at positions $N/2 - R$ and $N/2 + R + 1$ respectively, and are connected by a string of electric field of length $2R + 1$. They are created by means of the nonlocal operator $\hat{M}_R$, defined as

$$\hat{M}_R \equiv (\hat{a}_{\frac{N}{2}-R}^\dagger + \hat{b}_{\frac{N}{2}-R})\left[\prod_{j=\frac{N}{2}-R}^{\frac{N}{2}+R}\hat{U}_j^\dagger\right](\hat{a}_{\frac{N}{2}+R+1} + \hat{b}_{\frac{N}{2}+R+1}^\dagger). \quad (2)$$

As a result, the initial state is $|\psi(t=0)\rangle = \mathcal{N}\hat{M}_R|\Omega\rangle$, where $\mathcal{N}$ is a normalization constant. The state has the extra energy $\approx(2R+1)+4\{x[(m/q)^2+2x]\}^{1/2}$ above the ground state energy. When R is a finite fraction of the system size, the initial state has an extensive extra energy. As a result, the evolution of $|\psi(t=0)\rangle$ under Eq. (1) should mostly be driven by high-energy excited states.

Confinement and string breaking.—We would expect the charges, initially created at distance $2R + 1$, to separate by stretching the electric-flux string up to a critical distance that only depends on the boson mass. There ultimately the string would break as a result of boson pair production from

the vacuum. After that, lighter mesons would propagate freely (similarly to the FSM case [30]). However, in the BSM we do not observe such a scenario. We only see a *partial* screening of the initial electric-field string, leading to a partial string breaking, even for massless bosons. Our observations can be explained using a semiclassical cartoon presented in Fig. 1 displaying four main features of the OED:

Confinement and slow dynamics induced by the partial screening of electric field: The electric-flux string creates a long-lived metastable state in the middle of the system that oscillates and contract inwards [12,84,87,88], reducing the velocity of charges and bending the initial light cone [83]. The rate of production of new bosons is not sufficient to completely screen the electric field, so that their light-cone bends as the charges slow down and eventually start refocusing. The two charges are thus confined again into an extended meson that wobbles at a well-defined frequency (Fig. 1).

String-inversion in the bulk: The string does not break, not even for massless bosons, but rather undergoes at least a pair of coherent oscillations (see also Ref. [14]). For lighter masses, we observe a string-inversion phenomenon and slow damping of it by the radiation of lighter mesons.

Mesons radiation, the two domains: While in the bulk the string contracts and expands periodically, at the boundaries the electric flux is partially screened and the string can break into pieces forming lighter mesons. They are free to escape the confined region and fly away with a constant velocity, creating two separate domains. We observe a core region where the bosons are confined (a confined domain), and an outer region where they escape in the form of lighter mesons (a deconfined domain). The radiation of lighter mesons slowly depletes the electric field and the cloud of bosons in the confined region.

Quantitative results about the lack of thermalization.— The cartoon in Fig. 1 tries to summarize the numerical results presented in Fig. 2. There we plot both the electric field ($\hat{L}_j$) on the left and the dynamical charges ($\hat{Q}_j$) on the right for two paradigmatic values $m/q = 0$ and 1.2 that together display all the phenomena we have listed previously. The dynamics is generated by acting with the operator $\hat{M}_{R=5}$ [Eq. (2)] on the vacuum of Eq. (1). In the massless scenario (top row of Fig. 2), we appreciate the *partial screening* of the electric field, visible in the bending of the bosons' light cone; the appearance of an *antistring* in the bulk of the system due to the *string inversion* at $t \simeq 2.5$; the *meson radiation* from the edges of the confined bulk starting around $t \gtrsim 4$. We also see that the confined core of bosons is gradually depleted and disappears for times around $t \simeq 10$.

As we increase the mass, we slowly move towards the heavy-bosons' scenario of $m/q = 1.2$ (bottom row of Fig. 2), where the radiation of free mesons is strongly suppressed and the confined core is basically surrounded
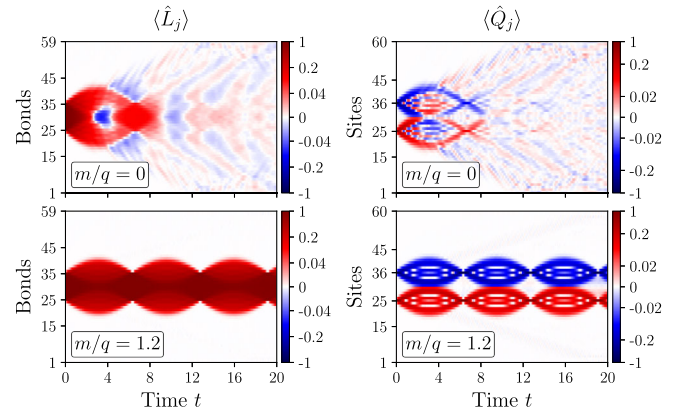

FIG. 2. Dynamics of the electric field $\hat{L}_j$ and the dynamical charge $\hat{Q}_j$ for $R = 5$.

by the vacuum. We indeed observe an almost perfect periodic oscillation of the electric string. Intermediate regimes (not shown, see Ref. [56]) display interesting features. For example for $m/q = 0.25$, the antistring, visible in $m/q = 0$ case, disappears and there is no string breaking for $m/q \gtrsim 0.5$.

While for $m/q = 0$ the concentration of dynamical charges in the confined domain gradually disappears for $t \gtrsim 10$, it persists in the asymptotic states for larger values of the mass. However, the confined core still lingers on for a long time, even in the massless case, which can be perceived through the fluctuation of $\hat{L}_j$ or $\hat{Q}_j$, or through the spreading of the entanglement entropy.

From the above discussions it is clear that confinement strongly hinders the thermalization process in the system and the "equilibrated" states are far from thermal.

Despite the qualitative difference in Fig. 2 between the light and heavy mass regime, we show now that they are both nonthermal and continuously connected. In Fig. 3(a), we consider the time-averaged fraction of the initial excess energy that leaks to the outer regions of the system. If the system eventually thermalizes the energy should spread uniformly (beside finite size boundary effects). In Fig. 3(a), the uniform value is represented by a red line, and different colors and symbols encode different time windows. The plot shows that for any time and value of m/q the energy stays trapped in the bulk as witnessed by the lower amount of energy leakage to the edges of the system than what is expected in an homogeneous system. Furthermore, the leakage continuously decreases as we increase m/q in a smooth way, without any transitions as shown by the perfect fit of our numerical data to the sigmoid curve $\sim 1/[1 + \exp(\nu m/q - c)]$ with exponent ν. For m/q larger than 1 the leaking is practically zero. There is thus a single dynamics regime characterized by a strong memory of the initial state.

The best way to characterize the slow dynamics is by considering the growth and spreading of entanglement.
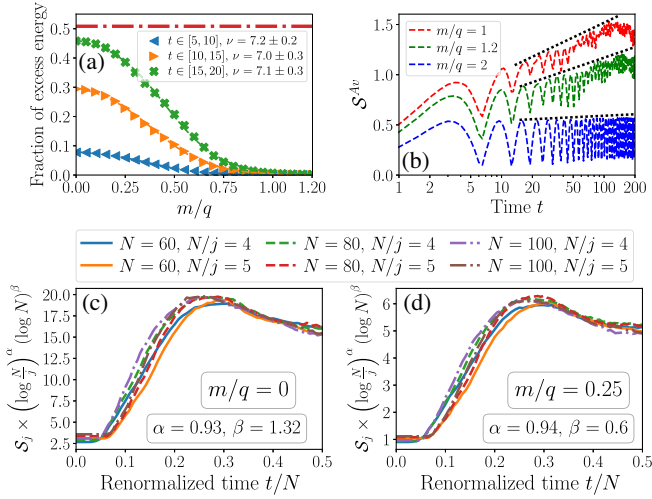
FIG. 3. (a) Time-averaged fraction of the initial extra energy that leaks from the core of the system towards the boundaries for different ratios of m/q and different time windows. We measure the excess energy across the bonds $[1, 15] \cup [45, 59]$ to obtain the fraction. The red dot-dashed line marks the ideal homogeneous value. The time-averaged fraction has been fitted by a sigmoid curve with exponent ν (see text). (b) Longtime behavior of the growth of entanglement entropy in the central region for larger values of masses. (c)–(d) Pattern of entanglement entropy in the deconfined domain for different systems and bipartition sizes for $m/q = 0$ (c) and 0.25 (d).

The entanglement entropy $\mathcal{S}_j$ measured across the bond between the sites j and $j+1$ is defined as $\mathcal{S}_j(t) = -\mathrm{Tr}[\rho_j(t) \ln \rho_j(t)]$, with $\rho_j(t) = \mathrm{Tr}_{j+1,j+2,\dots,N} |\psi(t)\rangle \langle \psi(t)|$ being the reduced density matrix to the left of the jth bond. The spread of entanglement out of equilibrium has been discussed originally in Ref. [98] and more recently in the context of generalized thermalization [4,91]. In the BSM, the spread of entanglement is strongly modified by the effect of confinement similar to the evolution of local observables mentioned earlier (see Ref. [56]).

We start analyzing the growth of entanglement entropy with time for larger masses as the simulations are less demanding [99]. By plotting the long time evolution of the average entropy in the central region, $\mathcal{S}^{Av} = [1/(2R + 1)] \sum_{j=N/2-R}^{N/2+R} \mathcal{S}_j$, we can appreciate how the entropy strongly oscillates with an envelope that grows logarithmically with time before saturating at $t \simeq 160$ [Fig. 3(b)]. Such a logarithmic growth of entropy bears a strong resemblance to observations in many-body-localized systems (MBL) [100,101]. Unlike in MBL, the saturated value of entanglement entropy does not depend on the system size (see Ref. [56]).

For lighter masses we cannot achieve such long times, but we can still analyze the scaling of the entropy with the system size in the asymptotic states we obtain. We consider $N = 60$, 80, and 100 and $R = N/10$, so that the length of the initial string grows proportional to the system size, thus

providing an extensive amount of energy on the top of the ground state and fulfilling one of the conditions for thermalization. In a thermalized system, the entropy of a region grows proportional to its size (volume law), while in the nonergodic scenario the entropy increases slower than that. We expect that the deconfined domain slowly becomes thermal, due to the radiation of lighter mesons, while the confined domain remains "nonthermal" showing coherent oscillations.

Indeed, in the confined domain the entropy shows a perfect area law dependence (see Ref. [56]). Neither its maximum value nor its average over the confined domain depend on the size of the region as shown in Ref. [56].

On the other hand, from the scaling plots [Figs. 3(c)–3(d)], we find that the entropy in the deconfined region varies as $\mathcal{S}_j \propto (\log[N/j])^{-\alpha} (\log N)^{-\beta}$, where the exponents $\alpha \approx 1$ and β depend on m/q. For fixed N, the entropy increases sublinearly for small bipartitions, then turns into a linear increase for intermediate distances, and ultimately shows faster than volume-law growth before saturating into the confined domain. From this scaling form, it seems reasonable to expect that the deconfined region would actually "thermalize" at intermediate distances, far away from both the core and the boundaries of the system. This complicated scaling form seems to match the behavior expected in a thermalized region with the presence of a physical boundary and of a confined core.

Classical and distillable entanglement dynamics.—As part of the gauge symmetry, the system possesses a global U(1) symmetry corresponding to the conservation of total dynamical charge, $\sum_j \hat{Q}_j$. As a result, any reduced density matrix is block diagonal in different charge sectors: $\rho = \bigoplus_Q \tilde{\rho}_Q = \bigoplus_Q p_Q \rho_Q$, where $p_Q = \mathrm{Tr}[\tilde{\rho}_Q]$ and $\rho_Q = \tilde{\rho}_Q / p_Q$. Therefore, following [102–109] the entanglement entropy can be divided into two parts as $\mathcal{S}(\rho) = -\sum_Q p_Q \ln p_Q + \sum_Q p_Q \mathcal{S}(\rho_Q)$, where the first term is the classical part ($\mathcal{S}^C$)—the Shannon entropy between different quantum blocks indicated by $Q \in [.., -1, 0, 1, ...]$, and the second term, the distillable entanglement ($\mathcal{S}^Q$) that has a clear operational significance [102].

Figure 4 shows the time evolution of both parts of the entanglement entropy. The classical part clearly demarcates confined and deconfined domains by remaining *sharply* concentrated only in the confined domain. Most of the bosons are confined in the core and thus populate several superselection sectors as witnessed by the large value of the classical entropy. In the deconfined domain, the density of lighter mesons that escape from the core is low, meaning that the only populated superselection sectors are $Q = 0$, ± 1. Furthermore, since mesons are short and dilute (on average we have less than one meson per site), $p_{Q=\pm 1} \ll p_{Q=0}$. We thus conclude that higher charge sectors are off-resonant in this domain, as they would require a higher density of mesons.
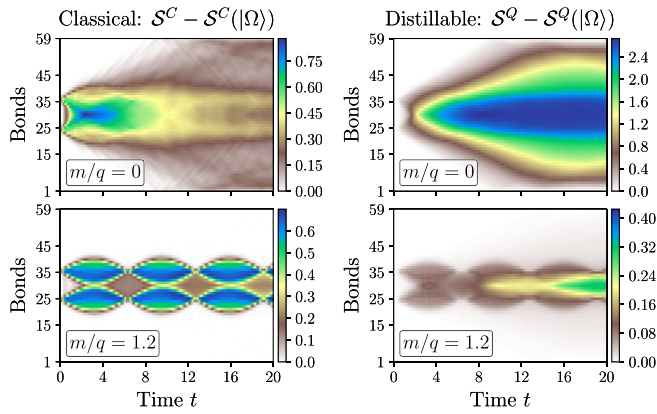
FIG. 4. Time evolution of the classical part $\mathcal{S}^C$ of entanglement entropy (left column) and the distillable entanglement entropy $\mathcal{S}^Q$ (right column). Here we subtract the corresponding entropies of the ground state $|\Omega\rangle$ and consider the case of $R = 5$.

The distillable part of the entropy spreads throughout the system in a "more ergodic" manner. It still retains a distinctly higher value in the confined domain within this timescale, but we believe it can be a finite time effect. Summarizing, the strong spatial inhomogeneity of the time-evolved entropies, especially of their classical part, gives us a clear generic signature of the lack of thermalization in the system.

Conclusion.—We have shown that the out-of-equilibrium dynamics generated by creating a pair of bosons on the top of the interacting vacuum of a gauge theory is strongly affected by confinement. The asymptotic states generated are highly inhomogeneous. They are made by a confined core that displays long-lived oscillations and entropically fulfills the area law, surrounded either by the vacuum (for heavy bosons) or by an almost thermal cloud of light mesons (for lighter bosons). In both cases, the long-time asymptotic states have a strong memory of the initial state and thus evade thermalization in its simplest form. The phenomena observed are reminiscent of the observations of the presence of highly nonthermal states in the quantum Ising model [13]. In a forthcoming paper [55] we will relate our findings to the intricate phase diagram of the BSM at equilibrium.

Interestingly, the initial confined core persists up to a very long time, as witnessed by the entanglement entropy. Indeed the best signature of this phenomenon is given by the spatial profile of the classical part of the entanglement entropy. We have pushed the current algorithms to their limit, and larger system size and times will have to be addressed either using the next generation of tensor-network methods (for recent proposal see Ref. [110] and references therein) or experimentally by quantum simulators [51].

Note added.—Recently, we became aware of a complementary approach that tries to explain the slow thermalization and the lack of thermalization observed in similar models in terms of fractons [111]. It will be interesting to understand if that approach can also be used here.

[*]titas.chanda@uj.edu.pl

[1] D. Fausti, R. I. Tobey, N. Dean, S. Kaiser, A. Dienst, M. C. Hoffmann, S. Pyon, T. Takayama, H. Takagi, and A. Cavalleri, Science **331**, 189 (2011).

[2] D. A. Abanin and Z. Papić, Ann. Phys. (Amsterdam) **529**, 1700169 (2017).

[3] F. Alet and N. Laflorencie, C. R. Phys. **19**, 498 (2018).

[4] M. Rigol, V. Dunjko, and M. Olshanii, Nature (London) **452**, 854 (2008).

[5] A. Polkovnikov, K. Sengupta, A. Silva, and M. Vengalattore, Rev. Mod. Phys. **83**, 863 (2011).

[6] J. Eisert, M. Friesdorf, and C. Gogolin, Nat. Phys. **11**, 124 (2015).

[7] L. D'Alessio, Y. Kafri, A. Polkovnikov, and M. Rigol, Adv. Phys. **65**, 239 (2016).

[8] E. Noether, Mathematisch-Physikalische Klasse **1918**, 235 (1918), https://eudml.org/doc/59024.

[9] O. A. Castro-Alvaredo, B. Doyon, and T. Yoshimura, Phys. Rev. X **6**, 041065 (2016).

[10] B. Bertini, M. Collura, J. De Nardis, and M. Fagotti, Phys. Rev. Lett. **117**, 207201 (2016).

[11] M. Brenes, M. Dalmonte, M. Heyl, and A. Scardicchio, Phys. Rev. Lett. **120**, 030601 (2018).

[12] N. J. Robinson, A. J. A. James, and R. M. Konik, Phys. Rev. B **99**, 195108 (2019).

[13] A. J. A. James, R. M. Konik, and N. J. Robinson, Phys. Rev. Lett. **122**, 130603 (2019).

[14] F. M. Surace, P. P. Mazza, G. Giudici, A. Lerose, A. Gambassi, and M. Dalmonte, arXiv:1902.09551.

[15] J. Park, Y. Kuno, and I. Ichinose, Phys. Rev. A **100**, 013629 (2019).

[16] A. C. Cubero and N. J. Robinson, arXiv:1908.00270.

[17] J. Schwinger, Phys. Rev. **82**, 664 (1951).

[18] J. Schwinger, Phys. Rev. **125**, 397 (1962).

[19] J. Schwinger, Phys. Rev. **128**, 2425 (1962).

[20] S. Coleman, Ann. Phys. (N.Y.) **101**, 239 (1976).

[21] C. Hamer, J. Kogut, D. Crewther, and M. Mazzolini, Nucl. Phys. **B208**, 413 (1982).

[22] C. Adam, Ann. Phys. (N.Y.) **259**, 1 (1997).

[23] T. V. Zache, N. Mueller, J. T. Schneider, F. Jendrzejewski, J. Berges, and P. Hauke, Phys. Rev. Lett. **122**, 050403 (2019).

[24] T. M. R. Byrnes, P. Sriganesh, R. J. Bursill, and C. J. Hamer, Phys. Rev. D **66**, 013002 (2002).

[25] M. Bañuls, K. Cichy, J. Cirac, and K. Jansen, J. High Energy Phys. 11 (2013) 158.

[26] B. Buyens, J. Haegeman, K. Van Acoleyen, H. Verschelde, and F. Verstraete, Phys. Rev. Lett. **113**, 091601 (2014).

[27] S. Kühn, J. I. Cirac, and M.-C. Bañuls, Phys. Rev. A **90**, 042305 (2014).

[28] M. C. Bañuls, K. Cichy, J. I. Cirac, K. Jansen, and H. Saito, Phys. Rev. D **92**, 034519 (2015).

[29] B. Buyens, F. Verstraete, and K. Van Acoleyen, Phys. Rev. D **94**, 085018 (2016).

[30] T. Pichler, M. Dalmonte, E. Rico, P. Zoller, and S. Montangero, Phys. Rev. X **6**, 011023 (2016).

[31] M. C. Bañuls, K. Cichy, J. I. Cirac, K. Jansen, and S. Kühn, Phys. Rev. Lett. **118**, 071601 (2017).

[32] E. Ercolessi, P. Facchi, G. Magnifico, S. Pascazio, and F. V. Pepe, Phys. Rev. D **98**, 074503 (2018).

[33] Y.-P. Huang, D. Banerjee, and M. Heyl, Phys. Rev. Lett. **122**, 250401 (2019).

[34] G. Magnifico, M. Dalmonte, P. Facchi, S. Pascazio, F. V. Pepe, and E. Ercolessi, arXiv:1909.04821.

[35] G. Delfino, G. Mussardo, and P. Simonetti, Nucl. Phys. **B473**, 469 (1996).

[36] G. Delfino and G. Mussardo, Nucl. Phys. **B516**, 675 (1998).

[37] G. Mussardo, J. High Energy Phys. 08 (2007) 003.

[38] D. González-Cuadra, P. R. Grzybowski, A. Dauphin, and M. Lewenstein, Phys. Rev. Lett. **121**, 090402 (2018).

[39] D. González-Cuadra, A. Dauphin, P. R. Grzybowski, P. Wójcik, M. Lewenstein, and A. Bermudez, Phys. Rev. B **99**, 045139 (2019).

[40] D. González-Cuadra, A. Bermudez, P. R. Grzybowski, M. Lewenstein, and A. Dauphin, Nat. Commun. **10**, 2694 (2019).

[41] K. Kasamatsu, I. Ichinose, and T. Matsui, Phys. Rev. Lett. **111**, 115303 (2013).

[42] O. Dutta, L. Tagliacozzo, M. Lewenstein, and J. Zakrzewski, Phys. Rev. A **95**, 053608 (2017).

[43] D. González-Cuadra, E. Zohar, and J. I. Cirac, New J. Phys. **19**, 063038 (2017).

[44] Y. Kuno, S. Sakane, K. Kasamatsu, I. Ichinose, and T. Matsui, Phys. Rev. D **95**, 094507 (2017).

[45] S. Nascimbène, Y.-A. Chen, M. Atala, M. Aidelsburger, S. Trotzky, B. Paredes, and I. Bloch, Phys. Rev. Lett. **108**, 205301 (2012).

[46] E. A. Martinez, C. A. Muschik, P. Schindler, D. Nigg, A. Erhard, M. Heyl, P. Hauke, M. Dalmonte, T. Monz, P. Zoller, and R. Blatt, Nature (London) **534**, 516 (2016).

[47] H. Bernien, S. Schwartz, A. Keesling, H. Levine, A. Omran, H. Pichler, S. Choi, A. S. Zibrov, M. Endres, M. Greiner, V. Vuletić, and M. D. Lukin, Nature (London) **551**, 579 (2017).

[48] N. Klco, E. F. Dumitrescu, A. J. McCaskey, T. D. Morris, R. C. Pooser, M. Sanz, E. Solano, P. Lougovski, and M. J. Savage, Phys. Rev. A **98**, 032331 (2018).

[49] F. Görg, K. Sandholzer, J. Minguzzi, R. Desbuquois, M. Messer, and T. Esslinger, Nat. Phys. **15**, 1161 (2019).

[50] C. Schweizer, F. Grusdt, M. Berngruber, L. Barbiero, E. Demler, N. Goldman, I. Bloch, and M. Aidelsburger, Nat. Phys. **15**, 1168 (2019).

[51] A. Mil, T. V. Zache, A. Hegde, A. Xia, R. P. Bhatt, M. K. Oberthaler, P. Hauke, J. Berges, and F. Jendrzejewski, arXiv:1909.07641.

[52] J. Kogut and L. Susskind, Phys. Rev. D **11**, 395 (1975).

[53] M. Creutz, Phys. Rev. D **15**, 1128 (1977).

[54] M. Creutz, I. J. Muzinich, and T. N. Tudron, Phys. Rev. D **19**, 531 (1979).

[55] T. Chanda, J. Zakrzewski, M. Lewenstein, and L. Tagliacozzo (to be published).

[56] See Supplemental Material at http://link.aps.org/supplemental/10.1103/PhysRevLett.124.180602 for the derivation of the discretized Hamiltonian and additional results, which includes Refs. [57–63].

[57] C. J. Hamer, Weihong Zheng, and J. Oitmaa, Phys. Rev. D **56**, 55 (1997).

[58] I. Kull, A. Molnar, E. Zohar, and J. I. Cirac, Ann. Phys. (Amsterdam) **386**, 199 (2017).

[59] S. Singh, R. N. C. Pfeifer, and G. Vidal, Phys. Rev. A **82**, 050301(R) (2010).

[60] S. Singh, R. N. C. Pfeifer, and G. Vidal, Phys. Rev. B **83**, 115125 (2011).

[61] S. R. White, Phys. Rev. B **72**, 180403(R) (2005).

[62] S. Goto and I. Danshita, Phys. Rev. B **99**, 054307 (2019).

[63] M. Hochbruck and C. Lubich, SIAM J. Numer. Anal. **34**, 1911 (1997).

[64] U. Schollwck, Ann. Phys. (Amsterdam) **326**, 96 (2011).

[65] F. Verstraete and J. I. Cirac, arXiv:cond-mat/0407066.

[66] R. Ors, Ann. Phys. (Amsterdam) **349**, 117 (2014).

[67] J. C. Bridgeman and C. T. Chubb, J. Phys. A **50**, 223001 (2017).

[68] S.-J. Ran, E. Tirrito, C. Peng, X. Chen, L. Tagliacozzo, G. Su, and M. Lewenstein, arXiv:1708.09213.

[69] G. M. Crosswhite, A. C. Doherty, and G. Vidal, Phys. Rev. B **78**, 035116 (2008).

[70] P. Hauke, F. M. Cucchietti, A. Müller-Hermes, M.-C. Bañuls, J. I. Cirac, and M. Lewenstein, New J. Phys. **12**, 113037 (2010).

[71] T. Koffel, M. Lewenstein, and L. Tagliacozzo, Phys. Rev. Lett. **109**, 267203 (2012).

[72] P. Hauke and L. Tagliacozzo, Phys. Rev. Lett. **111**, 207202 (2013).

[73] A. Milsted, J. Haegeman, and T. J. Osborne, Phys. Rev. D **88**, 085030 (2013).

[74] M. P. Zaletel, R. S. K. Mong, C. Karrasch, J. E. Moore, and F. Pollmann, Phys. Rev. B **91**, 165112 (2015).

[75] M. C. Bañuls, K. Cichy, J. I. Cirac, K. Jansen, and S. Kühn, Phys. Rev. X **7**, 041046 (2017).

[76] S. Paeckel, T. Köhler, A. Swoboda, S. R. Manmana, U. Schollwöck, and C. Hubig, Ann. Phys. (Amsterdam) **411,** 167998 (2019).

[77] T. Sugihara, J. High Energy Phys. 07 (2005) 022.

[78] L. Tagliacozzo and G. Vidal, Phys. Rev. B **83,** 115127 (2011).

[79] L. Tagliacozzo, A. Celi, and M. Lewenstein, Phys. Rev. X **4,** 041024 (2014).

[80] P. Silvi, E. Rico, T. Calarco, and S. Montangero, New J. Phys. **16,** 103015 (2014).

[81] S. Kühn, E. Zohar, J. I. Cirac, and M. C. Bañuls, J. High Energy Phys. 07 (2015) 130.

[82] J. Haegeman, K. Van Acoleyen, N. Schuch, J. I. Cirac, and F. Verstraete, Phys. Rev. X **5,** 011024 (2015).

[83] M. Kormos, M. Collura, G. Takcs, and P. Calabrese, Nat. Phys. **13,** 246 (2017).

[84] B. Craps, E. Lindgren, and A. Taliotis, J. High Energy Phys. 12 (2015) 1.

[85] J. Abajo-Arrastia, E. da Silva, E. Lopez, J. Mas, and A. Serantes, J. High Energy Phys. 05 (2014) 126.

[86] E. da Silva, E. Lopez, J. Mas, and A. Serantes, J. High Energy Phys. 04 (2015) 38.

[87] E. da Silva, E. Lopez, J. Mas, and A. Serantes, J. High Energy Phys. 06 (2016) 172.

[88] R. C. Myers, M. Rozali, and B. Way, J. Phys. A **50,** 494002 (2017).

[89] C. J. Turner, A. A. Michailidis, D. A. Abanin, M. Serbyn, and Z. Papić, Nat. Phys. **14,** 745 (2018).

[90] P. Sala, T. Rakovszky, R. Verresen, M. Knap, and F. Pollmann, Phys. Rev. X **10,** 011047 (2020).

[91] L. Vidmar and M. Rigol, J. Stat. Mech. (2016) 064007.

[92] M. E. Peskin and D. V. Schroeder, *An Introduction to Quantum Field Theory* (Addison-Wesley Pub. Co, Reading, Mass, 1995).

[93] S. R. White, Phys. Rev. Lett. **69,** 2863 (1992).

[94] S. R. White, Phys. Rev. B **48,** 10345 (1993).

[95] U. Schollwöck, Rev. Mod. Phys. **77,** 259 (2005).

[96] J. Haegeman, J. I. Cirac, T. J. Osborne, I. Pižorn, H. Verschelde, and F. Verstraete, Phys. Rev. Lett. **107,** 070601 (2011).

[97] J. Haegeman, C. Lubich, I. Oseledets, B. Vandereycken, and F. Verstraete, Phys. Rev. B **94,** 165116 (2016).

[98] P. Calabrese and J. Cardy, J. Stat. Mech. (2005) P04010.

[99] For larger masses, we are able to faithfully simulate the dynamics upto much longer time-scales, as entropy increases much slowly.

[100] M. Žnidarič, T. Prosen, and P. Prelovšek, Phys. Rev. B **77,** 064426 (2008).

[101] J. H. Bardarson, F. Pollmann, and J. E. Moore, Phys. Rev. Lett. **109,** 017202 (2012).

[102] N. Schuch, F. Verstraete, and J. I. Cirac, Phys. Rev. Lett. **92,** 087904 (2004).

[103] N. Schuch, F. Verstraete, and J. I. Cirac, Phys. Rev. A **70,** 042310 (2004).

[104] W. Donnelly, Phys. Rev. D **85,** 085004 (2012).

[105] D. Radicevic, arXiv:1404.1391.

[106] H. Casini, M. Huerta, and J. A. Rosabal, Phys. Rev. D **89,** 085012 (2014).

[107] H. Casini, M. Huerta, J. M. Magan, and D. Pontello, J. High Energy Phys. 02 (2020) 014.

[108] A. Lukin, M. Rispoli, R. Schittko, M. E. Tai, A. M. Kaufman, S. Choi, V. Khemani, J. Léonard, and M. Greiner, Science **364,** 256 (2019).

[109] P. Sierant, K. Biedro, G. Morigi, and J. Zakrzewski, SciPost Phys. **7,** 8 (2019).

[110] J. Surace, M. Piani, and L. Tagliacozzo, Phys. Rev. B **99,** 235115 (2019).

[111] S. Pai and M. Pretko, Phys. Rev. Research **2,** 013094 (2020).